Biophysical Journal, Volume *112*

Supplemental Information

Force Responses and Sarcomere Dynamics of Cardiac Myofibrils Induced by Rapid Changes in [P_i]

Robert Stehle

SUPPORTING MATERIAL

Force responses and sarcomere dynamics of cardiac myofibrils induced by rapid changes in [P_i]

Robert Stehle

Institute of Vegetative Physiology, University of Köln, Robert Koch Str. 39, D-50931 Cologne, Germany, e-mail: Robert.Stehle@Uni-Koeln.de

SUPPORTING METHODS

A thin bundle consisting of 2 to ~6 single myofibrils was stuck at one of its ends to the tip of a stiff tungsten needle (# 5775, A-M Systems, Inc., Carlsborg, WA) that was connected via a piezo actuator (P-821.20, Physik Instr., Karlsruhe, Germany) to a micromanipulator. After sticking the bundle to the needle, the free end of the bundle was moved to the tip of a atomic force cantilever (PPM-FM, Nanosensors™, Neuchatel, Switzerland). The tip was coated with a mixture (1:1 v/v) of silicon glue (3140 RTV Coating, Dow Corning, Midland, USA) and 4 % nitrocellulose in amyl-acetate. The end of the bundle was then pushed against the coating using a needle mounted on another micromanipulator. Bundles were visualized under bright field illumination using a long working distance objective lens (60x/0.70 Ph2 LCPlanFL, Olympus) and the 1.5x magnifier of the Olympus IX-70 microscope and imaged on an ORCA-ER camera (Hamamatsu Photonics, Japan). Bundles had diameters of 1.5–3.0 µm and slack lengths of 40–110 µm. Slack sarcomere length (sSL) was 2.02 ± 0.04 µm (mean ± SD). Prior activation, bundles were stretched to a sarcomere length (SL) of 2.3 µm.

Force changes were induced by a rapid solution change technique (1) with modifications as described in (2). In addition, three-barrel square-style capillaries were used instead of the two-barrel theta-style capillaries to allow the different changeover protocols. The capillaries were pulled to produce tip openings of the channels of ~100 µm and then bent by a micro-forge to provide parallel outflows of the solution streams relative to the bottom of the experimental chamber that was manufactured from a cover slip. Three adjacent laminar streams could be generated by gravitational pressure flowing continuously from the capillary and perpendicular to the myofibril axis. One stream contained a relaxing solution the other two activating solutions with different [P_i]. At the beginning of the experiment, the capillary was adjusted by using a micromanipulator to fully expose the myofibril to the stream of relaxing solution. During the experiment, the capillary was rapidly moved in lateral direction using a piezo actuator (P289.40, Physik Instr., Karlsruhe, Germany) to first expose the myofibril into the second stream and then to the third stream. The 1st move was used to increase the [Ca^{2+}] and the 2nd move to change the [P_i] during Ca^{2+}-activation. Subsequently, myofibrils were exposed again to the second and the first stream to reverse the [P_i]-change and to finally induce relaxation. The total time for each actuator movement (switch time) was set at 10 ms. The solution change at the myofibril occurred relative to the actuator movement with a delay of 10–25 ms, depending on the gravitational pressure for the flow (30–40 cm H_20) and the distance between pipette and myofibril (0.4–0.6 mm). A function consisting of an initial square term followed by a linear term and a second square term was used to drive the actuator position during the switchover. The square terms provided a constant acceleration and deceleration to prevent oscillations of the capillary by acceleration peaks that would produce perturbations of the flow profiles. The time of the effective solution change at the myofibril bundle was indicated by a peak- or sinusoidal-like artefact in the force signal arising from optical deflections of the laser beam when the bent flow profile passes the cantilever (2). This indicated a time for changeover of adjacent solutions of ~ 10 ms which allows measurements of rate constants of < 100 s^{-1} which is well below the observed kinetics of force changes upon stepping-up or stepping-down of [Ca^{2+}] or [P_i]. To characterize the kinetics of force redevelopment (k_{TR}-measurements), rapid length changes were applied to the myofibril using the P-821.20 piezo actuator. The myofibril was slackened by 15 % of its length for 100 ms and then re-stretched to the original length whereupon the force redevelops by a single exponential with rate constant k_{TR}.

DESCRIPTION OF SUPPORTING VIDEO DATA

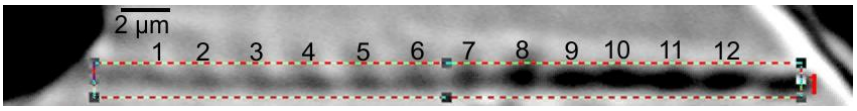

Movie S1A and S1B. Sarcomere dynamics following a rapid increase of [P_i] from 0.16 mM to 5 mM. *(Movie S1A)* The rectangle (green-red dashed line, also visible in the video) marks the region of interest (ROI) selected for evaluating the data shown in Fig. 3A (see Methods). The black numbers in the image on top (not depicted in the movie) indicate the sarcomeres analyzed for length changes according to the numbering of SL traces in Fig. 3A. During experiment, frames were sampled at intervals of 17.3 ms. The movie consists of 169 frames and starts 3 frames before the [P_i]-increase that occurs at frame 4. To better follow in the movie the fast sarcomere dynamics, it was stored on the databank in 2-fold slow motion, i.e., the original duration of the movie was 2.9 s before it was stretched to 5.8 s. *(Movie S1B)* For a closer view of sarcomeres analyzed within the ROI, the movie *S1A* was cut to the ROI and 2-fold magnified in size. Sarcomere ´give´ initiates in the movies at sarcomere #12 and propagates to the left.

Movie S2: Sarcomere ´give´ and subsequent SPOC after increase of [P_i] from 0.16 mM to 20 mM. During experiment, frames were sampled at intervals of 41.1 ms. The movie consists of 120 frames and starts 3 frames before the increase of [P_i] that occurs at frame 4 of the movie. The movie stored on the databank shows the sequence in 2-fold slow motion i.e., movie time was stretched from 4.9 s to 9.8 s. The movie illustrates the pronounced sarcomere dynamics at high [P_i]. Sarcomere ´give´ initiates at the right side near the cantilever and propagates to the left. When ´give´ reaches the left end of the bundle, it restarts at the right side resulting in a continuous SPOC wave.

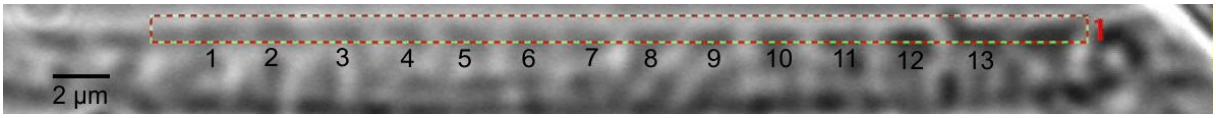

Movie S3A and S3B. Sarcomere dynamics following a rapid decrease of [P_i] from 20 mM to 5 mM. *(Movie S3A)* The rectangle (green-red dashed line, also visible in the movie) marks the region of interest (ROI) selected for evaluating the data shown in Fig. 4C. The black numbers in the image on top (not depicted in the movie) indicate the sarcomeres analyzed for length changes according to the numbering of SL traces in Fig. 4C. Note that due to the axial shift of sarcomeres between single myofibrils only a distal part of the bundle and only 13 of the 19 sarcomeres in total could be quantitatively analyzed. During experiment, frames were sampled at intervals of 19.9 ms. The movie consists of 150 frames and starts 3 frames before the [P_i]-decrease that occurs at frame 4. The movie stored on the databank shows the sequence in 2-fold slow motion i.e., movie time was stretched from 3.0 s to 6.0 s. (*Movie S3B*) For a closer view of the sarcomeres, the movie *S3A* was cut to the ROI and 2-fold magnified in size. As seen in the movies, there is inhomogeneous shortening of sarcomeres but neither rapid lengthening of individual sarcomeres (´give´) nor organized sarcomere dynamics.

SUPPORTING MODEL SIMULATIONS

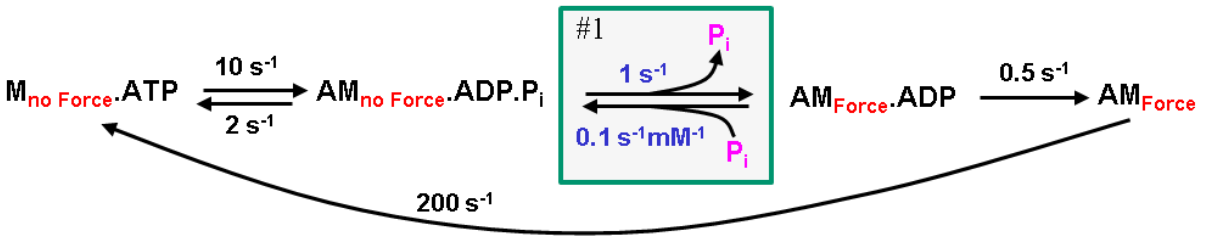

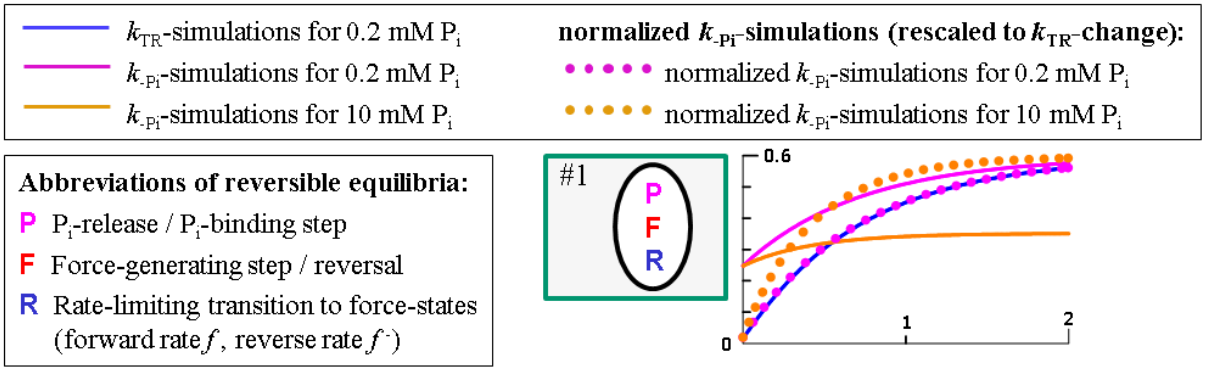

Fig S1: **Simulated force transients after rapid decrease of [P_i] and upon mechanically-induced force redevelopment for different model scenarios.**

Description of model simulations in Fig S1: Force kinetics upon rapid $[P_i]$-changes and in k_{TR}-experiment were simulated by 11 different versions of a model, created by completing the same basic model (shown on top) with each one of the 11 numbered green-marked modules. For the sake of clarity, the modules are given in abbreviated form. Only the first module is also depicted in its explicit form which refers to the green marked equilibrium embedded in the basic model on top. Values for rate constants of ATP-cleavage (10 s^{-1}, reverse rate 2 s^{-1}) and ATP-binding induced cross-bridge detachment from actin (200 s^{-1}) were estimated from kinetics of intrinsic tryptophan fluorescence and P_i-bursts observed upon mixing guinea pig cardiac myofibrils in rigor with MgATP in a stopped-flow and a stopped-flow-quench apparatus, respectively (Stehle, unpublished data). The rate constant that limits the forward turnover of cross-bridges from force-generating to non-force states (termed *g*) is assigned to the transition from the ADP-binding to the rigor state, assuming ATP-binding and ATP-induced dissociation to be much faster. The value of *g* for isometric conditions (0.5 s^{-1}) refers to the rate constant k_{LIN} of isometric relaxation as well as to k_{TR} measured at low Ca^{2+}-activations and low $[P_i]$ (0.2 mM). In model #1, the forward rate constants and the reverse rate constants of the P_i-release (reversible equilibrium P) and the force-generating step (reversible equilibrium F) are merged with the forward rate constant f and the reverse rate constant f^- of the rate-limiting transition (reversible equilibrium R) for forward and reverse turnover of cross-bridges from non-force to force-generating states, respectively. The value of 1.0 s^{-1} for f was estimated by subtracting *g* from the value of k_{TR} determined at high $[Ca^{2+}]$ (pCa 4.5) and low $[P_i]$ (0.2 mM). The value of 0.10 $s^{-1}mM^{-1}$ for f^- was estimated from the slopes of the linear increases of k_{TR}, k_{-Pi}, and $k_{+Pi(1)}$ versus the $[P_i]$ (data in manuscript, Fig.´s 2B and 4B).

To search for model scenarios with faster kinetics of phosphate release or/and force-generating step than the rate-limiting transition able to describe the observed force kinetics upon $[P_i]$-change, the three reversible equilibria (P, F, and R) merged in model version #1 were split up by inserting additional states within the modules (abbreviated by □) and making forward steps and reverse steps for P or/and F faster than those for R. Encircling of F or P with R indicates that F or P, respectively, remains merged with R. When fastened, forward and reverse rate of the equilibrium was increased in parallel and kept equal to maintain reactions reversible. Graphs next to each module show corresponding simulations for the case of 10-fold faster kinetics of P and F compared to R. To simulate 10-fold faster kinetics of P in model versions #2, #3, and #6 to #11, the forward (dissociation) rate constant $k_{P(D)}$ of P was set at 10 s^{-1} and the reverse (binding) rate constant $k_{P(B)}$ changed to 1 $s^{-1}mM^{-1}$; the rate constants f and f^- of R were set at 1 s^{-1}. To simulate 10-fold faster kinetics of F in model versions #4 to #11, the forward rate constant k_F and the reverse rate constant k_R were set at 10 s^{-1}. Simulated force transients are plotted on a time scale of 2 s upon perturbation of $[P_i]$ or *g* at $t = 0$. For k_{-Pi}-simulations (pink and orange), $[P_i]$ was decreased from 20 mM to 0.2 mM (pink line) or from 20 mM to 10 mM (orange line). For k_{TR}-simulations at a constant $[P_i]$ of 0.2 mM (blue line), *g* was changed from a high value (50 s^{-1}) for unloaded shortening back to the low value of 0.5 s^{-1} for the isometric condition. Numbers on y-axis indicate the fraction of cross-bridges in force-states for the lined data. For better comparison of kinetics, k_{-Pi}-simulations are also shown in normalized form (dots in corresponding colors), by rescaling them to the same amplitude and shifting them to the same initial value obtained for the k_{TR}-simulation in the corresponding model version. Comparison of normalized k_{-Pi}-simulations at 0.2 mM P_i (pink dots) with the k_{TR}-simulation at 0.2 mM P_i (blue line) illustrates the similarity or deviation between k_{-Pi} and k_{TR}. Comparison between normalized k_{-Pi}-simulations at 0.2 mM P_i (pink dots) and 10 mM P_i (orange dots) illustrates the effect of $[P_i]$ on kinetics. Noteworthy, in all the different model versions, simulations always yielded the same kinetics when $[P_i]$ is increased (not illustrated) or decreased to same final $[P_i]$, i.e. all models predict symmetric kinetics.

As indicated by the similar kinetics in k_{-Pi} and k_{TR}-simulations (pink dots versus blue lines), model version #1 in which P_i-release and force-generating step are inseparable from the transition limiting *f*, model versions #2 and #3 in which a rate-limiting force-generating step occurs before or after phosphate release, and model versions #4 and #5 in which a fast force-generating step occurs before or after a rate-limiting P_i-release, can account for the observed slow force kinetics induced by $[P_i]$-change and the observed similarity of k_{-Pi} to k_{TR}. However, model versions #1, #2 and #3 imply that *any* changes in occupancy of force-generating states are slow, like k_{-Pi}, k_{TR} and k_{ACT}. This is inconsistent with the phenomenon of rapid force recovery upon rapid length change that has been proposed to probe the force-generating step(s) (3). Hence, model versions #1 to #3 fail to combine the slow force kinetics induced by $[P_i]$ with the fast force kinetics induced by rapid length changes, unless slow force generation in k_{TR}-experiments or upon rapid increase in $[P_i]$ reflect a different force generating mechanism than quick tension recovery (4). In contrast, model versions #4 and #5 can account for both observations. Clearly, classical model versions in which the transition limiting *f* precedes a fast force-generating step that leads (model version #6) or follows (model version #7) a rapid P_i-release yield a force rise upon $[P_i]$-change that is markedly faster than the force rise simulated for the k_{TR}-experiment (compare pink dots with blue lines) which is inconsistent with the observed slow force response upon $[P_i]$-change in myofibril experiments. Models in which a fast force-generating step prior (model version #8) or subsequent (model version #9) to a rapid P_i-release precede the rate-limiting transition produce similar fast kinetics in k_{-Pi} and k_{TR}-simulations but yield a high occupancy of force-generating states during the phase of unloaded shortening, i.e. a high duty ratio at v_{max} as indicated by the high initial values of the blue lines (note that the y-axis starts at different values in the model versions). This is a problem common to all models in which the force-generating step occurs before the step limiting *f* and concerns also model versions #4 and #10. The high duty ratios at v_{max} of > 30% predicted by the model versions #4, #8, #9 and #10 (note that for these models, the y-axes start at ≥ 0.3) are very unlikely because of the low fraction of strongly-bound cross-bridges at v_{max} determined by fiber stiffness measurements which indicate a duty ratio of less than 5 % (5). Separating the fast force-generating step from the fast P_i-release by inserting a slow transition between the two fast steps (model versions #10 and #11) yield slow force kinetics upon $[P_i]$-changes but are incompatible with the observed changes in force and force kinetics when $[P_i]$ is changed. Thus, in model version #10, force becomes insensitive to the $[P_i]$ and in model version #11, force kinetics do not become faster but slower at increasing $[P_i]$. Note that model version #1 yields the highest modulation of force and force kinetics by $[P_i]$ while model version #5 can best combine the slow force kinetics upon change in $[P_i]$ with the fast force recovery upon rapid length steps and a low duty ratio during unloaded shortening. This would mean that P_i-release controls a rate-limiting transition (or vice versa) prior to a fast force-generating step. However, if the rapid force recovery reflects a mechanism of force-generation different from that reflected by k_{TR} and k_{-Pi} (6), then model versions #1, #2 and #3 are also possible. In this case, force kinetics upon $[P_i]$-change cannot reveal whether the force-generating step occurs before (model version #2), along (#1) or after (#3) P_i-release. In any case, the scenario of a fast force-generating step coupled to a fast P_i-release (or vice versa), i.e. model versions #6 and #7, can be excluded.

SUPPORTING REFERENCES

1. Colomo, F., S. Nencini, …, C. Tesi. 1998. Calcium dependence of the apparent rate of force generation in single striated muscle myofibrils activated by rapid solution changes. *Adv. Exp. Med. Biol.* 453:373-381.

2. Stehle, R., M. Krüger, …, G. Pfitzer. 2002. Isometric force kinetics upon rapid activation and relaxation of mouse, guinea pig and human heart muscle studied on the subcellular myofibrillar level. *Basic Res. Cardiol.* 97:I127-135.

3. Huxley, A. F., and R. M. Simmons. 1971. Proposed mechanism of force generation in striated muscle. *Nature.* 233:533-538.

4. Brenner, B., J. M. Chalovich, and L. C. Yu. 1995. Distinct molecular processes associated with isometric force generation and rapid tension recovery after quick release. *Biophys. J.* 68:106S-111S.

5. Stehle, R., and B. Brenner. 2000. Cross-bridge attachment during high-speed active shortening of skinned fibers of the rabbit psoas muscle: implications for cross-bridge action during maximum velocity of filament sliding. *Biophys. J.* 78:1458-1473.

6. Brenner, B. 1991. Rapid dissociation and reassociation of actomyosin cross-bridges during force generation: a newly observed facet of cross-bridge action in muscle. *Proc. Natl. Acad. Sci. USA* 88:10490-10494.